Research Article

Nano Research
2024, 17(5): 3700–3706

ISSN 1998-0124 CN 11-5974/O4
https://doi.org/10.1007/s12274-023-6271-0

Long-range Pt-Ni dual sites boost hydrogen evolution through optimizing the adsorption configuration

Cong Liu[1], Pengfang Zhang[2] (✉), Bing Liu[3], Qian Meng[2], Xuzhao Yang[1], Yakun Li[1], Jingli Han[1], and Yao Wang[3] (✉)

[1] *Henan Province Engineering Research Center of Catalysis and Separation of Cyclohexanol, College of Materials and Chemical Engineering, Zhengzhou University of Light Industry, Zhengzhou 450001, China*
[2] *Shandong Provincial Key Laboratory of Chemical Energy Storage and Novel Cell Technology, Liaocheng University, Liaocheng 252000, China*
[3] *Key Laboratory of Synthetic and Biological Colloids, Ministry of Education, School of Chemical and Material Engineering, International Joint Research Center for Photoresponsive Molecules and Materials, Jiangnan University, Wuxi 214122, China*

Received: 29 September 2023 / **Revised:** 13 October 2023 / **Accepted:** 15 October 2023

ABSTRACT

Elaborated design of catalytic systems with a specifically tailored site distance to match the intermediates could substantially improve reaction kinetics and boost catalytic activity under unfavorable reaction conditions. Considering the lower energy barriers of water splitting upon the synergy of dual sites, constructing synergistic Pt-M (M: transition metal) dual sites is an effective way to boost Pt with highly catalytic hydrogen evolution reaction (HER) performance. An unconventional "$Ni(OH)_2$-coated high-index Pt facets" was constructed to obtain long-range Pt-Ni dual sites, in which Ni composition as a water dissociation synergistic site can protect Pt from electrolyte corrosion and ensure efficient proton donation to Pt sites. The obtained long-range Pt-Ni dual sites present 3.84 $mA \cdot cm^{-1}$ of current density, which is 7.5 times specific activity higher than that of commercial Pt/C towards alkaline HER. The enhanced HER performance is attributed to synergistic catalysis on Pt-Ni dual sites accompanied by unconventional electron coupling. This work illustrates a new strategy to construct the long-range dual sites by unconventional strategy for fundamental electrocatalytic study of alkaline HER.

KEYWORDS

long-range, Pt-Ni dual sites, electron transfer, hydrogen evolution reaction, sites synergy

1 Introduction

Hydrogen (H_2), as a clean and renewable energy resource, has been considered as a promising candidate instead of fossil fuel [1–5]. In order to produce hydrogen, water-electrolysis in alkaline environment has received a lot of attention because of its enormous advantages including adequate reactants, persistent products, and high product purity [6–12]. Today, Pt-based catalysts are long believed to own the highest activity towards hydrogen evolution reaction (HER) among enormous reported electrocatalysts [13–16]. However, the sluggish reaction kinetics of HER in alkaline environment is about 2–3 orders of magnitude lower than that in acidic solution, and the intrinsic mechanisms of HER process are indistinct and divergent [17–22].

In this case, constructing dual sites for accelerating the bond-breaking of H–OH molecule is a promising strategy to boost HER performance [23–26]. N. M. Markovic [27] and co-workers revealed that Ni modified single-crystal Pt sites featured boosted HER performance, and the further exploration disclosed that the improved performance can be given the credit to the interfacial electronic synergy of Pt-Ni dual sites for hydrogen recombination. Simultaneously modulating the surface coordination environment of synergistic sites and rational engineering the electron structure of Pt and Ni dual sites are dominant and beneficial for improving the HER activity. However, in the practical HER process [28, 29], alloyed Pt-M (M: transition metal) dual sites are insufficient for an excellent performance towards HO–H bond-breaking. Drawbacks remain that M atoms inserted into Pt crystalline lattice are prone to be assimilated by adjacent Pt atoms and hardly play prominent effect as additional participants during HER process [30, 31]. Thus, enlarging the interatomic distance of Pt-M dual sites can bring out the best in them through electron transfer and site synergy [32–35]. So, fabricating the long-range dual sites [36–39] is an effective approach to exploiting their synergistic effect on HER.

Herein, we proposed a strategy by coating $Ni(OH)_2$ on high-index Pt facets (HIFs) to construct long-range Pt-Ni dual sites, which not only increase the numbers of long-range Pt-Ni dual sites, but also engineer the physico-chemical property of Pt and Ni. The obtained Pt-Ni dual sites show a 3.84 $mA \cdot cm^{-1}$ of current density, which is 7.5 times specific activity higher than those of commercial Pt/C towards HER in alkaline solution. The boosted HER performance is put down to synergistic catalysis of Pt-Ni dual sites accompanied by unconventional electron coupling. Thus, designing an advanced catalyst by constructing $Ni(OH)_2$ coated Pt HIFs is important to fundamental understanding of the synergistic effect of long-range Pt-Ni dual sites that account for HER enhancement.

Address correspondence to Pengfang Zhang, zhangpengfang@lcu.edu.cn; Yao Wang, wangyao@jiangnan.edu.cn

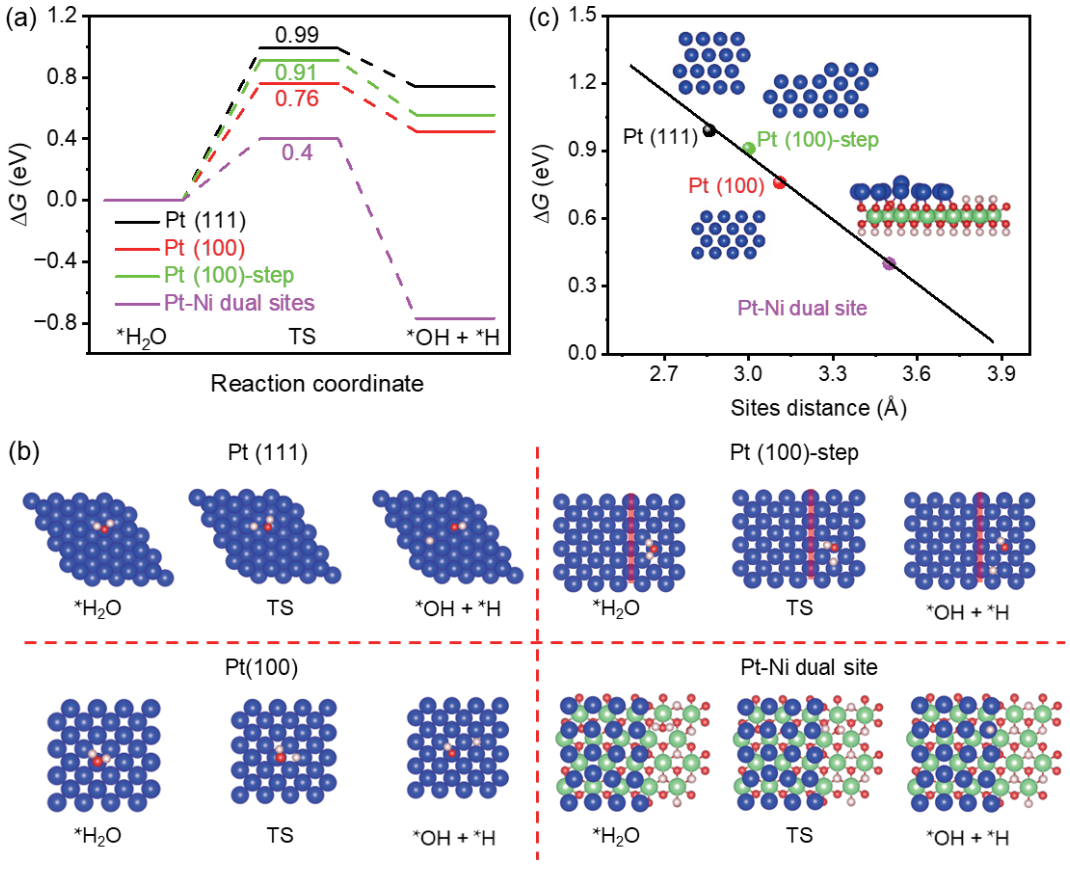

Figure 1 (a) Energy profiles of the water dissociation process and (b) the geometries of the initial, transition and final states on bare Pt (111), Pt (100), Pt (100)-step, and Pt-Ni dual sites matrix. (c) A plot is constructed from computational calculated Gibbs free energy of different sites distance. Blue: Pt, green: Ni, white: O, red: H.

2 Results and discussion

To verify this assumption and supply a theoretical guidance for this dual site catalyst, we performed density functional theory (DFT) to model the rate determining step (H–OH bond-breaking) for alkaline HER. First, the energy barriers (ΔG) of water dissociation process on three different Pt surfaces: Pt (111), Pt (100), Pt (100)-step, and Pt-Ni dual sites were calculated (Fig. S1 in the Electronic Supplementary Material (ESM)), with the purpose of expounding the facilitation of active site distance acted on alkaline HER. As shown in Figs. 1(a) and 1(b), the ΔG for bond-breaking of HO–H in water molecule are 0.99, 0.91, 0.76, and 0.40 eV on Pt (111), Pt (100)-step, Pt (100), and Pt-Ni dual sites, respectively. It is obviously seen that the Pt-Ni dual sites show the lowest ΔG for water dissociation, indicating Pt-Ni dual sites are in favor of HO–H bond-breaking. In comparison with Pt (100) surface, the Pt (100)-step shows a higher ΔG of water dissociation, which demonstrates that the boosting effect of undercoordinated Pt (100) sites on H–OH bond-breaking is inferior to non-stepped Pt (100) sites. However, in the previous report, Pt (111)-step shows a lower ΔG of water dissociation compared with Pt (111) surface. Thus, it inspired us to further explore the intrinsic nature for Pt (111) and Pt (100) surface sites that account for the boosted HER performance. Figure 1(c) shows a plot of sites distance of different surface structures and the combinations with ΔG. It is shown that the ΔG of water dissociation keeps a linear relationship with dual sites distance within limits. The site distance of Pt-Ni dual sites owning an optimum performance is about 3.5 Å, which demonstrates that the long-range Pt-Ni dual sites can be well matched with the intermediates via optimizing the adsorption configurations.

Apart from site synergy of long-range Pt-Ni dual sites, the electron coupling is also considered to reveal the promoting effect on HO–H bond-breaking. The Pt (100) plane is placed on the $Ni(OH)_2$ nanosheets (Pt (100)@$Ni(OH)_2$, Fig. S2 in the ESM) as a reference catalyst to investigate the electron effect on Pt sites. The ΔG of water dissociation on Pt (100)@$Ni(OH)_2$ is about 0.61 eV, lower than that of Pt (100) sites, indicating that the electron coupling of Pt and $Ni(OH)_2$ is beneficial for HO–H bond-breaking. Combining with the results of Pt-Ni dual sites, the low ΔG of water dissociation can be attributed to the electron effect and synergistic effect of long-range Pt-Ni dual sites.

To verify our theoretical predictions, we designed two types of catalysts: concave nanocube Pt and $Ni(OH)_2$-coated concave nanocube Pt (long-range Pt-Ni dual sites). The as-defined Pt nanocrystals were fabricated according to our previous report [40]. As shown in Fig. 2(a), the transmission electron microscopy (TEM) image shows that the as-obtained Pt nanoparticles are concave cubic shape with uniform dispersion, which can be further revealed by high-angle annular dark-field scanning TEM (HAADF-STEM) image (Fig. 2(b)). Meanwhile, the average diameter size (apex-to-apex) of Pt nanocrystals is about 44.1 nm with high morphology selectivity above 90% (Fig. 2(a), inset). Particle size distribution of the synthesized monodisperse nanoparticles was acquired by counting a minimum of 100 particles from different regions of the sample from TEM image. Figure 2(c) exhibits clear surface steps in individual Pt particle characterized by high-evolution TEM (HRTEM). The corresponding fast Fourier transform (FFT) pattern (Fig. 2(c), top-right inset) revealed that the HRTEM is obtained along the [100] zone axis. Thus, the angles between the facets of Pt nanocrystals could be definitely measured and used to determine the facet indices. The facet angles are measured approximately 10°, 12°, 14°, and 16°, keeping pace with the calculated values (Fig. S4 in the ESM) of {610}, {510}, {410}, and {720} facets. Thus, the Pt nanocrystals are covered by typical HIFs. The corresponding models are shown in Fig. S5 in the ESM.

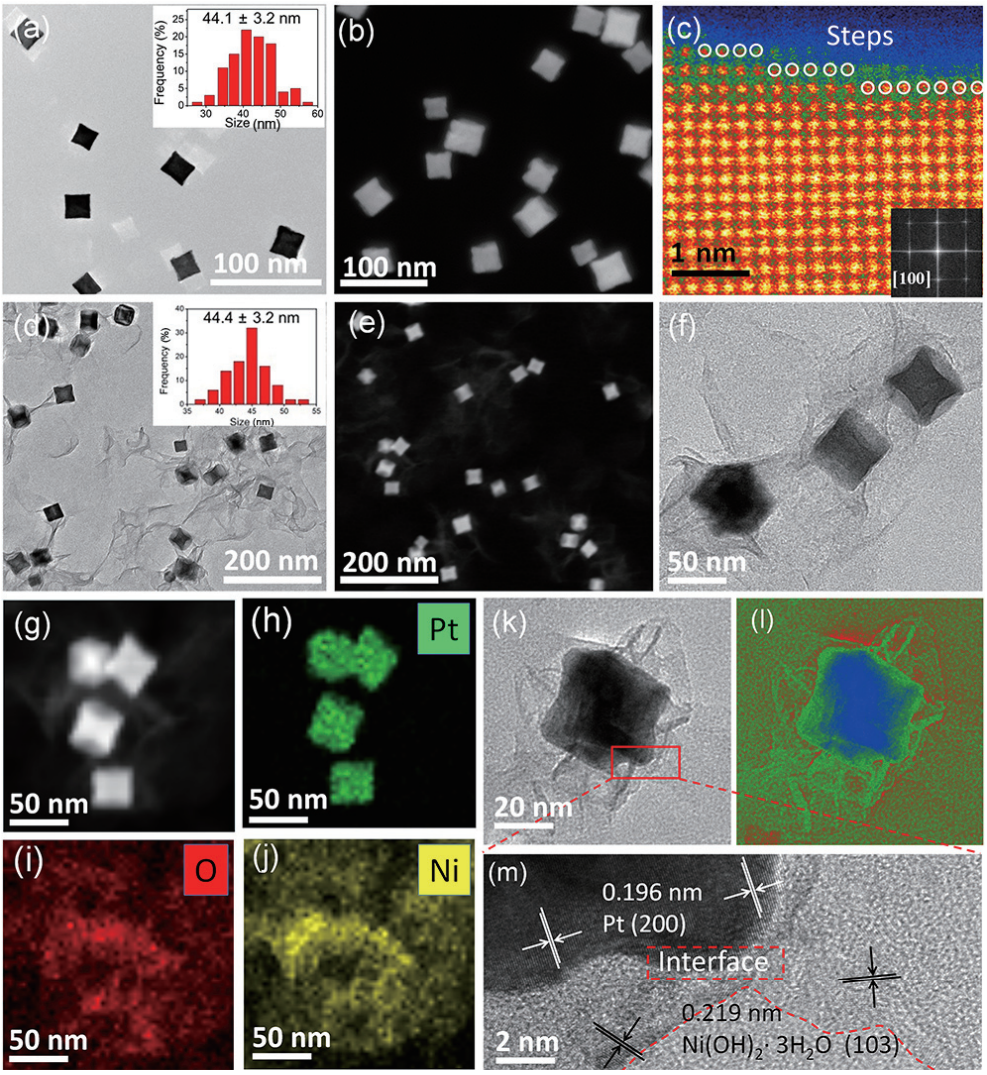

Figure 2 (a) TEM and size distribution histogram, (b) HAADF-STEM, (c) HRTEM images of as-defined Pt nanoparticles. ((d) and (f)) TEM image, (e) HAADF-STEM image of Pt-Ni dual sites. ((g)–(j)) Nanoscale elemental mappings of Pt-Ni dual sites. (k) TEM image of Pt-Ni dual sites. (l) False color was applied in the TEM images to improve the contrast. (m) HRTEM image of Pt-Ni dual sites.

The long-range Pt-Ni dual sites were successfully prepared by wet-chemical method for the first time. As shown in Fig. 2(d), the coated Pt nanoparticles by membrane-like $Ni(OH)_2$ can be clearly observed, which can be further demonstrated by HAADF-STEM image (Fig. 2(e)), in which the bright interior core is Pt nanocrystals and the surrounding dark domains are $Ni(OH)_2$ membranes (Fig. 2(f)). It is noted that the size of particles has nearly hardly changed. Nanoscale element mappings (Figs. 2(g)–2(j)) show that Pt, O, and Ni are uniformly dispersed in Pt-Ni dual sites.

The striking contrast of Pt core and $Ni(OH)_2$ membranes could be further observed based on the isolated particle in Figs. 2(k) and 2(l). Furthermore, the HRTEM was carried out to reveal the intimate interface structure between Pt core and $Ni(OH)_2$ membranes. As shown in Fig. 2(m), it is clearly observed that $Ni(OH)_2$ membranes grow on the surface of Pt particles, forming an abundant intimate contact. The lattice distances with interplanar spacings are 0.196 and 0.219 nm, corresponding to the (200) plane of Pt and (103) plane of $Ni(OH)_2{\cdot}3H_2O$ crystal phase, respectively.

It is noted that, in this work, N,N-dimethylformamide (DMF) plays an important role in fabricating successfully Pt-Ni dual sites. In the second step of preparation process, when the mixture of cyclohexane and DMF was replaced by pure cyclohexane, the segregated Pt particles and $Ni(OH)_2$ nanosheets were obtained, as shown in Fig. S6 in the ESM. Thus, it can be referred that the treating process can adjust the pH value of the solution to govern the hydrolysis of Ni^{2+} at a certain rate [41], which can not only avoid the local agglomeration of $Ni(OH)_2$, but also promote its uniform growth to coat on the Pt particles.

The Pt-Ni dual sites were characterized by X-ray diffraction (XRD). Figure 3(a) shows the XRD patterns of the as-prepared Pt and Pt-Ni dual sites, of which the well-defined Pt particles own a highly crystalline face-centered cubic (fcc) Pt phase. The Pt nanocrystal features the highest {111} and {200} peak intensities. After hybriding $Ni(OH)_2$ composition, the crystalline positions of Pt nanocrystals in Pt-Ni dual sites can keep pace with the pure Pt, disclosing that the modification of $Ni(OH)_2$ does not change the crystal structure of Pt nanocrystals. In addition, it is observed that the peaks located at 58° and 75° for Pt-Ni dual sites are the typical crystal structure of $Ni(OH)_2$, demonstrating the presence of $Ni(OH)_2$ composition.

X-ray photoelectron spectroscopy (XPS) was carried out to detect the surface chemical constituents and information of long-range Pt-Ni dual sites. Figure 3(b) exhibits the Pt 4f peaks of the Pt and Pt-Ni dual sites. The Pt 4f spectra of two catalysts present that the main components of the surface Pt are in the metallic state. The signals of Pt $4f_{7/2}$ in Pt and Pt-Ni dual sites are 70.72 and 71.02 eV, respectively. The configurations in the Pt 4f XPS spectra for Pt-Ni dual sites indicate a positive shift compared with Pt,

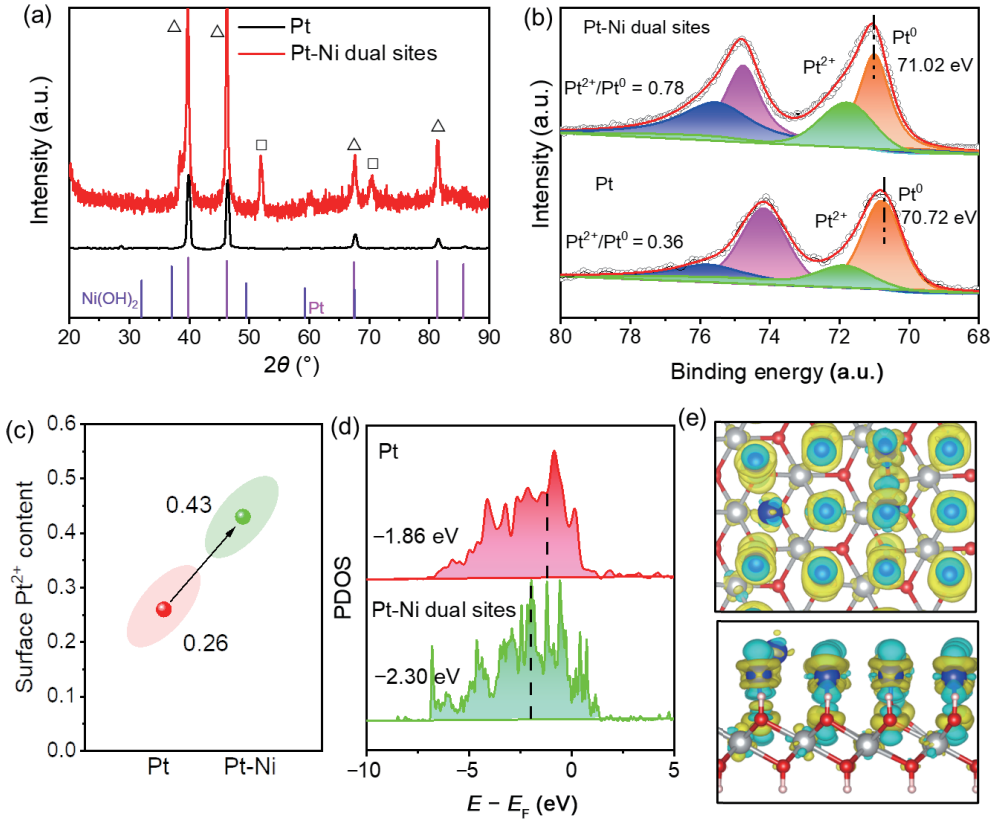

Figure 3 (a) XRD patterns (Δ: $Ni(OH)_2$, □: Pt) and (b) XPS spectra of Pt and Pt-Ni dual sites. (c) Surface Pt^{2+} content of Pt and Pt-Ni dual sites (surface Pt^{2+} content: $Pt^{2+}/(Pt^0 + Pt^{2+})$). (d) The PDOS of surface Pt atoms and d-band center positions of Pt and Pt-Ni dual site models. (e) The charge density difference of Pt-Ni dual sites (top view and side view).

which ultimately involved an optimization of Pt d-band center [42, 43]. From the deconvolutions of the Pt 4f signals, the signal centered at 71.89 eV, attributing to Pt^{2+} component from the passivated Pt–O layer [44]. It is clearly seen that the ratio of $Pt^{2+}/(Pt^0 + Pt^{2+})$ increased from the 0.26 to 0.43 (Fig. 3(c)) after introducing the $Ni(OH)_2$ composite, which is resulted from intensive electron transfer from Pt to $Ni(OH)_2$. The electronic interactions of Pt and $Ni(OH)_2$ were further assessed by theoretical modelling. As shown in Fig. 3(d), it is seen that the binding energy of the Pt d-orbital in Pt-Ni dual sites changes from −1.86 to −2.30 eV in comparison with Pt from the plot of the projected d-density of states (PDOSs), which is in favor of the water splitting. The electronic redistribution of Pt in the Pt-Ni dual sites steered by the electron cloud coupling can be clearly presented in Fig. 3(e), revealing an unconventional electron movement around the Pt-Ni dual sites. The above electronic behavior discloses a strong electronic interaction for Pt and Ni dual sites. Simultaneously, the electron localization function analysis (Fig. S7 in the ESM) demonstrates the delocalization level of electron interface around Pt-Ni dual sites.

The HER performance of the Pt-Ni dual sites was evaluated by typical electrochemical workstation. And commercial Pt/C (20 wt.%) was also tested as a standard under the same testing benchmark. The cyclic voltammetry (CV) was first employed to calculate the electrochemical surface area (ECSA) values of Pt and Pt-Ni dual sites catalysts and commercial Pt/C in alkaline solution. As shown in Fig. S8 in the ESM, the ECSA values of Pt and Pt-Ni dual sites tested in alkaline media (0.1 M KOH) are about 14.6 and 11.9 $m^2 \cdot g^{-1}$. The lower ECSA value of Pt-Ni dual sites indicates that core–shell structure of Pt-Ni dual sites would cover some active sites of Pt.

The HER performance of as-obtained Pt-Ni dual sites was tested in 0.1 M KOH solution. The commercial Pt/C was also measured as a reference. In general, the specific activities of Pt, Pt-Ni dual sites, and commercial Pt/C were assessed on the basis of ECSA (Fig. S8 in the ESM). It is obviously seen from the Figs. 4(a) and 4(b) that the specific activities (at 0.07 V vs. reversible hydrogen electrode (RHE)) of Pt-Ni dual sites and Pt are 3.84 and 2.46 $mA \cdot cm^{-2}$, respectively, which are 7.5 and 4.8 times higher than that of Pt/C (0.51 $mA \cdot cm^{-2}$). In addition, the mass activities of all catalysts were also measured according to real-loading of Pt on the electrode. As seen from Fig. 4(b), the mass activity of Pt-Ni dual sites is 0.52 $mA \cdot cm^{-2}$, which is 5.2 times higher than that of commercial Pt/C (0.1 $mA \cdot mg^{-1}$). The high HER activity of Pt-Ni dual sites is attributed to its intrinsic surface structure of encapsulated structure. First, possessing amounts of undercoordinated surface Pt atoms can provide abundant active sites for adsorbing water molecule, which was demonstrated that defect Pt sites are in favor of higher HER activity because of lower ΔG for water dissociation. Second, Pt-Ni dual sites possess abundant intimate interface of defect Pt sites and defective $Ni(OH)_2$ nanosheets, of which the water dissociation can be expedited via the synergistic catalysis of long-range Pt-Ni dual sites via decreasing the ΔG of water splitting.

The Tafel slope is an intrinsic nature of electrocatalysts, relating to the rate-limiting step of HER. The Tafel slope can be calculated by the Tafel equation ($\eta = a + b\log j$, where j indicates the current density, b indicates the Tafel slope, a indicates the intercept, and η indicates the overpotential) [45, 46]. The mechanism of HER [24, 47] in basic solution is traditionally considered as a combination of three main reactions: Volmer reaction ($2H_2O + M + 2e^- \leftrightarrows 2M\text{-}H_{ad} + 2OH^-$ (120 mV)), followed by the Heyrovsky reaction ($H_2O + H_{ad}\text{-}M + e^- \leftrightarrows M + H_2 + OH^-$ (40 mV)), or the Tafel reaction ($2M\text{-}H_{ad} \leftrightarrows 2M + H_2$ (30 mV)). In both the Volmer–Heyrovsky reaction and the Volmer–Tafel reaction, the first step is H–OH bond-cleavage. Figure 4(c) shows the Tafel slope of Pt-Ni dual sites, Pt, and commercial Pt/C. The Tafel slope values are 37.2, 66.4, and 48.6 $mV \cdot dec^{-1}$ for Pt-Ni dual sites, Pt, and commercial

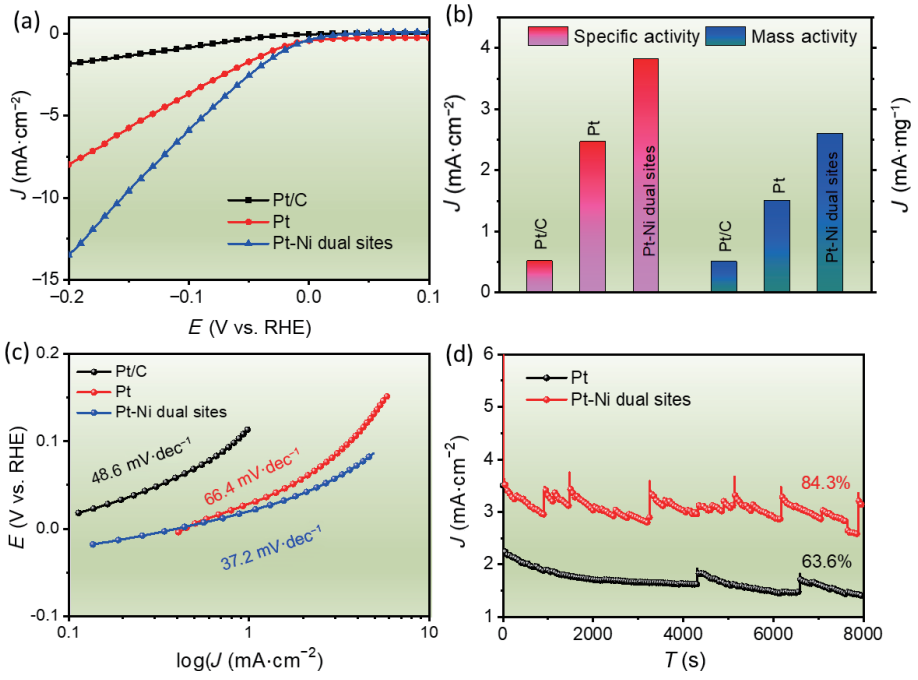

Figure 4 (a) HER curves, (b) specific activities and mass activities, and (c) Tafel slope driving from polarization curves of commercial Pt/C, Pt, and Pt-Ni dual sites. (d) Normalized current–time (*i*–*t*) chronoamperometric responses of Pt and Pt-Ni dual sites.

Pt/C, which demonstrate that the primary discharge (Volmer step) is the rate-limiting step for Pt-Ni dual sites. In addition, it is noted that after introducing the Ni sites, the Tafel slope of Pt decreases from 66.4 to 37.2 mV·dec^{-1}, revealing that the existence of $Ni(OH)_2$ can optimize the Volmer reaction steps and lower the reaction ΔG. The stability of Pt-Ni dual sites was assessed by chronoamperometric measurements. Figure 4(d) shows that the well-defined Pt-Ni dual sites keep 84.3% of initial activity after 8000 s test, which is higher than the activity of Pt (63.6%) catalyst. The enhanced HER durability further reveals that of Ni sites has a benefit on stabilizing the surface structure of Pt sites. As we know, the high surface free energy of HIFs is detrimental for long-term measurements because the surface stepped metal atoms are easy to dissociate and migrate. The introduction of Ni can delay this trend of irreversible evolution, which was further identified by TEM images after stability tests (Fig. S9 in the ESM).

An excellent performance dominantly depends on the matching degree between active sites and reaction intermediates in the field of catalysis. Thus, expounding the structure-performance relationship of long-range Pt-Ni dual sites is necessary for advancing the fundamental study in nanoscience and nanocatalysis. Thus, after the detailed discussion based on above characterizations, the enhanced performance of HER should be attributed to electronic effect and synergistic effect based on long-range Pt-Ni dual sites. In terms of electronic effect, it is noted that after introducing the Ni, the binding energy of Pt has a positive shift in comparison with pure Pt (XPS results), which will cause an optimizing adsorption behavior between catalyst and intermediates, facilitating a performance enhancement. Apart from the electronic effect, the synergistic effect also plays an important role in improving HER activity. Illustrated in Fig. 5, the combination of long-range Ni site and Pt site will provide amounts of atomic interfaces, in which the adsorbed H_2O molecule will be decomposed via the co-adsorption behavior that H_{ad} is adsorbed on Pt and OH_{ad} is adsorbed on the Ni, leading to a repaid water dissociation process [24].

3 Conclusions

In summary, a novel strategy that constructing synergistic long-range Pt-Ni dual sites to match the intermediates was proposed to accelerate the HO–H bond-cleavage of H_2O molecule. The $Ni(OH)_2$ coated Pt nanocrystals with HIFs were successfully constructed by using Pt nanocrystals as grow template. It is the first report of fine engineering of Pt nanocrystals with HIFs@hydroxide membranes composite, of which the Pt is well modified by $Ni(OH)_2$ membranes. The obtained Pt-Ni dual sites show a 7.5 times specific activity and 5.2 times mass activity higher than those of Pt/C towards basic HER. The improved HER performance (activity and stability) is attributed to the electronic

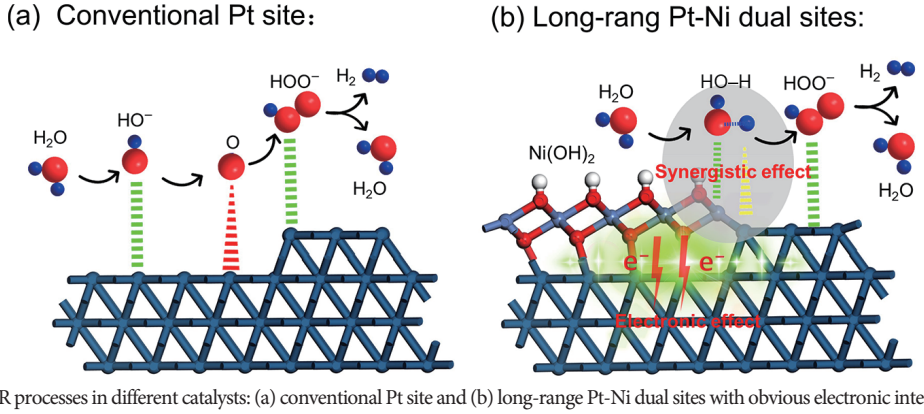

Figure 5 Illustrated HER processes in different catalysts: (a) conventional Pt site and (b) long-range Pt-Ni dual sites with obvious electronic interactions.

effect and synergistic effect of long-range Pt-Ni dual sites. This work develops a new avenue to steer the electronic behavior of long-range dual sites with outstanding electrocatalytic performance for alkaline HER and beyond.

Acknowledgements

This work was supported by the National Natural Science Foundation of China (No. 22305101), the Natural Science Foundation of Jiangsu Province (No. BK20231032), the Fundamental Research Funds for the Central Universities (No. JUSRP123020), Doctoral Science Research Foundation of Zhengzhou University of Light Industry (No. 2021BSJJ008), the Scientific and Technological Project of Henan Province (Nos. 222102240079, 232102230139, and 212102210209), and Henan Province College Students Innovation Project (No. 202310462017).

Electronic Supplementary Material: Supplementary material (detail experimental section, computational details, and linear sweep voltammetry (LSV) curves) is available in the online version of this article at https://www.doi.org/10.1007/s12274-023-6271-0.

References

[1] Dubouis, N.; Grimaud, A. The hydrogen evolution reaction: From material to interfacial descriptors. *Chem. Sci.* **2019**, *10*, 9165–9181.

[2] Hua, W.; Sun, H. H.; Xu, F.; Wang, J. G. A review and perspective on molybdenum-based electrocatalysts for hydrogen evolution reaction. *Rare Met.* **2020**, *39*, 335–351.

[3] Wang, B.; Yang, F. L.; Feng, L. G. Recent advances in Co-based electrocatalysts for hydrogen evolution reaction. *Small*, in press, https://doi.org/10.1002/smll.202302866.

[4] Zhou, W. J.; Jia, J.; Lu, J.; Yang, L. J.; Hou, D. M.; Li, G. Q.; Chen, S. W. Recent developments of carbon-based electrocatalysts for hydrogen evolution reaction. *Nano Energy* **2016**, *28*, 29–43.

[5] Gan, T.; Wang, D. S. Atomically dispersed materials: Ideal catalysts in atomic era. *Nano Res*, in press, https://doi.org/10.1007/s12274-023-5700-4.

[6] Lu, Q. P.; Yu, Y. F.; Ma, Q. L.; Chen, B.; Zhang, H. 2D transition-metal-dichalcogenide-nanosheet-based composites for photocatalytic and electrocatalytic hydrogen evolution reactions. *Adv. Mater.* **2016**, *28*, 1917–1933.

[7] Meng, X. Y.; Yu, L.; Ma, C.; Nan, B.; Si, R.; Tu, Y. C.; Deng, J.; Deng, D. H.; Bao, X. H. Three-dimensionally hierarchical MoS_2/graphene architecture for high-performance hydrogen evolution reaction. *Nano Energy* **2019**, *61*, 611–616.

[8] Puangsombut, P.; Tantavichet, N. Effect of plating bath composition on chemical composition and oxygen reduction reaction activity of electrodeposited Pt-Co catalysts. *Rare Met.* **2019**, *38*, 95–106.

[9] Turner, J. A. Sustainable hydrogen production. *Science* **2004**, *305*, 972–974.

[10] Yin, H. J.; Tang, Z. Y. Ultrathin two-dimensional layered metal hydroxides: An emerging platform for advanced catalysis, energy conversion and storage. *Chem. Soc. Rev.* **2016**, *45*, 4873–4891.

[11] Zhu, J.; Hu, L. S.; Zhao, P. X.; Lee, L. Y. S.; Wong, K. Y. Recent advances in electrocatalytic hydrogen evolution using nanoparticles. *Chem. Rev.* **2020**, *120*, 851–918.

[12] Shen, J.; Wang, D.S. How to select heterogeneous CO_2 reduction electrocatalyst. *Nano Research Energy*, in press, https://doi.org/10.26599/NRE.2023.9120096.

[13] Bender, J. T.; Petersen, A. S.; Østergaard, F. C.; Wood, M. A.; Heffernan, S. M. J.; Milliron, D. J.; Rossmeisl, J.; Resasco, J. Understanding cation effects on the hydrogen evolution reaction. *ACS Energy Lett.* **2023**, *8*, 657–665.

[14] Wu, S. H.; Li, C.; Wang, Y.; Zhuang, Y.; Pan, Y.; Wen, N.; Wang, S.; Zhang, Z. Z.; Ding, Z. X.; Yuan, R. S. et al. The Keto-switched photocatalysis of reconstructed covalent organic frameworks for efficient hydrogen evolution. *Angew. Chem., Int. Ed.* **2023**, *62*, e202309026.

[15] Yoo, S. H.; Aota, L. S.; Shin, S.; El-Zoka, A. A.; Kang, P. W.; Lee, Y.; Lee, H.; Kim, S. H.; Gault, B. Dopant evolution in electrocatalysts after hydrogen oxidation reaction in an alkaline environment. *ACS Energy Lett.* **2023**, *8*, 3381–3386.

[16] Wang, F. Q.; Zhang, W. L.; Wan, H. B.; Li, C. X.; An, W. K.; Sheng, X.; Liang, X. Y.; Wang, X. P.; Ren, Y. L.; Zheng, X. et al. Recent progress in advanced core-shell metal-based catalysts for electrochemical carbon dioxide reduction. *Chin Chem Lett* **2022**, *33*, 2259–2269.

[17] Zheng, J.; Sheng, W. C.; Zhuang, Z. B.; Xu, B. J.; Yan, Y. S. Universal dependence of hydrogen oxidation and evolution reaction activity of platinum-group metals on pH and hydrogen binding energy. *Science* **2016**, *2*, e1501602.

[18] Sheng, W. C.; Zhuang, Z. B.; Gao, M. R.; Zheng, J.; Chen, J. G.; Yan, Y. S. Correlating hydrogen oxidation and evolution activity on platinum at different pH with measured hydrogen binding energy. *Nat. Commun.* **2015**, *6*, 5848.

[19] Tang, P.; Huang, P. Y.; Swallow, J. E. N.; Wang, C. B.; Gianolio, D.; Guo, H.; Warner, J. H.; Weatherup, R. S.; Pasta, M. Structure-property relationship of defect-trapped Pt single-site electrocatalysts for the hydrogen evolution reaction. *ACS Catal.* **2023**, *13*, 9558–9566.

[20] Wang, L.; Liu, Y. N.; Chen, Z. F.; Dai, Q. Z.; Dong, C. L.; Yang, B.; Li, Z. J.; Hu, X. B.; Lei, L. C.; Hou, Y. Theory-guided design of electron-deficient ruthenium cluster for ampere-level current density electrochemical hydrogen evolution. *Nano Energy* **2023**, *115*, 108694.

[21] Yang, W. W.; Li, M. Y.; Zhang, B. K.; Liu, Y. Z.; Zi, J. Z.; Xiao, H.; Liu, X. Y.; Lin, J. K.; Zhang, H. Y.; Chen, J. et al. Interfacial microenvironment modulation boosts efficient hydrogen evolution reaction in neutral and alkaline. *Adv. Funct. Mater.*, in press, https://doi.org/10.1002/adfm.202304852.

[22] Zheng, X. Z.; Shi, X. Y.; Ning, H. H.; Yang, R.; Lu, B.; Luo, Q.; Mao, S. J.; Xi, L. L.; Wang, Y. Tailoring a local acid-like microenvironment for efficient neutral hydrogen evolution. *Nat. Commun.* **2023**, *14*, 4209.

[23] Wang, L.; Zhu, Y. H.; Zeng, Z. H.; Lin, C.; Giroux, M.; Jiang, L.; Han, Y.; Greeley, J.; Wang, C.; Jin, J. Platinum-nickel hydroxide nanocomposites for electrocatalytic reduction of water. *Nano Energy* **2017**, *31*, 456–461.

[24] Wang, P. T.; Zhang, X.; Zhang, J.; Wan, S.; Guo, S. J.; Lu, G.; Yao, J. L.; Huang, X. Q. Precise tuning in platinum-nickel/nickel sulfide interface nanowires for synergistic hydrogen evolution catalysis. *Nat. Commun.* **2017**, *8*, 14580.

[25] Ning, S.; Ou, H.; Li, Y.; Lv, C.; Wang, S.; Wang, D.; Ye, J. Co^0–$Co^{\delta+}$ interface double-site-mediated C–C coupling for the photothermal conversion of CO_2 into light olefins. *Angew. Chem., Int. Ed.* **2023**, *62*, e202302253.

[26] Wang, L. G.; Wu, J. B.; Wang, S. W.; Liu, H.; Wang, Y.; Wang, D. S. The reformation of catalyst: From a trial-and-error synthesis to rational design. *Nano Res*, in press, https://doi.org/10.1002/smll.202302866.

[27] Subbaraman, R.; Tripkovic, D.; Chang, K.-C.; Strmcnik, D.; Paulikas, A. P.; Hirunsit, P.; Chan, M.; Greeley, J.; Stamenkovic, V.; Markovic, N. M. Trends in activity for the water electrolyser reactions on 3d M (Ni, Co, Fe, Mn) hydr(oxy)oxide catalysts. *Nat. Mater.* **2012**, *11*, 550–557.

[28] Li, M. F.; Duanmu, K. N.; Wan, C. Z.; Cheng, T.; Zhang, L.; Dai, S.; Chen, W. X.; Zhao, Z. P.; Li, P.; Fei, H. L. et al. Single-atom tailoring of platinum nanocatalysts for high-performance multifunctional electrocatalysis. *Nat. Catal.* **2019**, *2*, 495–503.

[29] Zhu, S. Q.; Qin, X. P.; Xiao, F.; Yang, S. L.; Xu, Y.; Tan, Z.; Li, J. D.; Yan, J. W.; Chen, Q.; Chen, M. S. et al. The role of ruthenium in improving the kinetics of hydrogen oxidation and evolution reactions of platinum. *Nat. Catal.* **2021**, *4*, 711–718.

[30] Wang, Y.; Wu, J.; Tang, S. H.; Yang, J. R.; Ye, C. L.; Chen, J.; Lei, Y. P.; Wang, D. S. Synergistic Fe-Se atom pairs as bifunctional oxygen electrocatalysts boost low-temperature rechargeable Zn-air battery. *Angew. Chem., Int. Ed.* **2023**, *62*, e202219191.

[31] Wang, Y.; Zheng, M.; Li, Y. R.; Ye, C. L.; Chen, J.; Ye, J. Y.; Zhang, Q. H.; Li, J.; Zhou, Z. Y.; Fu, X. Z. et al. p-d orbital hybridization induced by a monodispersed ga site on a Pt_3Mn nanocatalyst boosts ethanol electrooxidation. *Angew. Chem., Int. Ed.* **2022**, *61*, e202115735.

[32] Qin, Y. C.; Zhang, W. L.; Wang, F. Q.; Li, J. J.; Ye, J. Y.; Sheng, X.; Li, C. X.; Liang, X. Y.; Liu, P.; Wang, X. P. et al. Extraordinary p-d hybridization interaction in heterostructural Pd-PdSe nanosheets boosts C–C bond cleavage of ethylene glycol electrooxidation. *Angew. Chem., Int. Ed.* **2022**, *61*, e202200899.

[33] Zheng, X. B.; Yang, J. R.; Li, P.; Jiang, Z. L.; Zhu, P.; Wang, Q. S.; Wu, J. B.; Zhang, E. H.; Sun, W. P.; Dou, S. X. et al. Dual-atom support boosts nickel-catalyzed urea electrooxidation. *Angew. Chem., Int. Ed.* **2023**, *62*, e202217449.

[34] Li, R. Z.; Zhang, Z. D.; Liang, X.; Shen, J.; Wang, J.; Sun, W. M.; Wang, D. S.; Jiang, J. C.; Li, Y. D. Polystyrene waste thermochemical hydrogenation to ethylbenzene by a N-bridged Co, Ni dual-atom catalyst. *J. Am. Chem. Soc.* **2023**, *145*, 16218–16227.

[35] Qin, Y. C.; Wang, F. Q.; Liu, P.; Ye, J. Y.; Wang, Q.; Wang, Y.; Jiang, G. C.; Liu, L. J.; Zhang, P. F.; Liu, X. B. et al. Enhancement of CH_3CO^* adsorption by editing d-orbital states of Pd to boost C–C bond cleavage of ethanol eletrooxidation. *Sci China Chem*, in press, https://doi.org/10.1007/s11426-023-1756-8.

[36] Li, W. H.; Yang, J.; Wang, D. Long-range interactions in diatomic catalysts boosting electrocatalysis. *Angew. Chem., Int. Ed.* **2022**, *61*, e202213318.

[37] Gao, Y.; Liu, B. Z.; Wang, D. S. Microenvironment engineering of single/dual-atom catalysts for electrocatalytic application. *Adv. Mater.* **2023**, *35*, 2209654.

[38] Hu, Y. M.; Chao, T. T. ; Li, Y. P.; Liu, P. G.; Zhao, T. H.; Yu, G.; Chen, C.; Liang, X.; Jin, H. L.; Niu, S. W. et al. Cooperative Ni(Co)-Ru-P sites activate dehydrogenation for hydrazine oxidation assisting self-powered H_2 production. *Angew. Chem., Int. Ed.* **2023**, *62*, e202308800.

[39] Zheng, X. B.; Yang, J. R,; Li, P.; Wang, Q. S.; Wu, J. B.; Zhang, E. H.; Chen, S. H.; Zhuang, Z. C.; Lai, W. H.; Dou, S. X.; Sun, W. P.; Wang, D. S.; Li, Y. D. Ir-Sn pair-site triggers key oxygen radical intermediate for efficient acidic water oxidation. *Sci. Adv*, **2023**, *9*, eadi8025.

[40] Wang, Y.; Zhuo, H. Y.; Sun, H.; Zhang, X.; Dai, X. P.; Luan, C. L.; Qin, C. L.; Zhao, H. H.; Li, J.; Wang, M. L. et al. Implanting Mo atoms into surface lattice of Pt_3Mn alloys enclosed by high-indexed facets: Promoting highly active sites for ethylene glycol oxidation. *ACS Catal.* **2019**, *9*, 442–455.

[41] Wang, P. T.; Shao, Q.; Cui, X. N.; Zhu, X.; Huang, X. Q. Hydroxide-membrane-coated Pt_3Ni nanowires as highly efficient catalysts for selective hydrogenation reaction. *Adv. Funct. Mater.* **2018**, *28*, 1705918.

[42] Cheng, R. Q.; Min, Y. L.; Li, H. X.; Fu, C. P. Electronic structure regulation in the design of low-cost efficient electrocatalysts: From theory to applications. *Nano Energy* **2023**, *115*, 108718.

[43] Huang, W. J.; Wang, H. T.; Zhou, J. G.; Wang, J.; Duchesne, P. N.; Muir, D.; Zhang, P.; Han, N.; Zhao, F. P.; Zeng, M. et al. Highly active and durable methanol oxidation electrocatalyst based on the synergy of platinum-nickel hydroxide-graphene. *Nat. Commun.* **2015**, *6*, 10035.

[44] Hunt, S. T.; Milina, M.; Wang, Z. S.; Román-Leshkov, Y. Activating earth-abundant electrocatalysts for efficient, low-cost hydrogen evolution/oxidation: Sub-monolayer platinum coatings on titanium tungsten carbide nanoparticles. *Energy Environ. Sci.* **2016**, *9*, 3290–3301.

[45] Kye, J.; Shin, M.; Lim, B.; Jang, J. W.; Oh, I.; Hwang, S. Platinum monolayer electrocatalyst on gold nanostructures on silicon for photoelectrochemical hydrogen evolution. *ACS Nano* **2013**, *7*, 6017–6023.

[46] Zhang, B.; Zhu, H.; Zou, M. L.; Liu, X. R.; Yang, H.; Zhang, M.; Wu, W. W.; Yao, J. M.; Du, M. L. Design and fabrication of size-controlled Pt-Au bimetallic alloy nanostructure in carbon nanofibers: A bifunctional material for biosensors and the hydrogen evolution reaction. *J. Mater. Sci.* **2017**, *52*, 8207–8218.

[47] Li, L. G.; Wang, P. T.; Shao, Q.; Huang, X. Q. Metallic nanostructures with low dimensionality for electrochemical water splitting. *Chem. Soc. Rev.* **2020**, *49*, 3072–3106.